



# Ceria-supported ruthenium clusters transforming from isolated single atoms for hydrogen production via decomposition of ammonia

Xiu-Cui Hu<sup>a</sup>, Xin-Pu Fu<sup>a</sup>, Wei-Wei Wang<sup>a</sup>, Xu Wang<sup>b</sup>, Ke Wu<sup>d</sup>, Rui Si<sup>b,\*</sup>, Chao Ma<sup>c,\*</sup>, Chun-Jiang Jia<sup>a,\*</sup>, Chun-Hua Yan<sup>d</sup>

<sup>a</sup> Key Laboratory for Colloid and Interface Chemistry, Key Laboratory of Special Aggregated Materials, School of Chemistry and Chemical Engineering, Shandong University, Jinan 250100, China

<sup>b</sup> Shanghai Synchrotron Radiation Facility, Shanghai Institute of Applied Physics, Chinese Academy of Sciences, Shanghai 201204, China

<sup>c</sup> College of Materials Science and Engineering, Hunan University, Changsha 410082, China

<sup>d</sup> Beijing National Laboratory for Molecular Sciences, State Key Lab of Rare Earth Materials Chemistry and Applications, PKU-HKU Joint Lab in Rare Earth Materials and Bioinorganic Chemistry, Peking University, Beijing 100871, China

## ARTICLE INFO

### Keywords:

Ru clusters  
Ceria  
Ammonia decomposition  
Hydrogen  
Structure-activity relation

## ABSTRACT

Supported cluster catalyst exhibits significant superiority in catalytic performance, but the structure uniformity and reactivity stability of the clusters under harsh conditions remains challenges. Here, we report the synthesis of stable ruthenium (Ru) clusters (ca. 1.5 nm) by reducing Ru single atoms under ammonia atmosphere at 550 °C, where the Ru clusters are uniformly dispersed on the surface of ceria. The supported Ru cluster catalysts show outstanding activity for decomposition of ammonia with an extremely high hydrogen yield of 9,924 mmolH<sub>2</sub> g<sub>Ru</sub><sup>-1</sup> min<sup>-1</sup> at 450 °C. Such a value exhibits at least one-order enhancement on the hydrogen formation yield compared to the previously reported results. Through comprehensive *in-situ* characterizations and temperature programmed desorption by NH<sub>3</sub> techniques, we clearly explored the structure-function relation of the Ru/CeO<sub>2</sub> catalyst that ceria support itself effectively adsorbed ammonia, meanwhile the Ru clusters stabilized by ceria decomposed ammonia to produce hydrogen.

## 1. Introduction

Supported metal cluster catalysts have attracted much attention in heterogeneous catalysis due to their unique features including high active species efficiency, strong metal-support interaction and unsaturated-coordination of active metal atoms [1–4]. While, a severe issue concerned for cluster catalysts is its bad structure uniformity and poor stability under harsh reaction conditions because of the sintering of active metal species. In recent years, space-confined strategy has been widely applied to stabilize the active species in the catalysts, such as the spatially controlled channel encapsulation [5,6] and the core-shell structure construction [7]. However, the synthesis of the encapsulated catalysts is generally complicated and the complex texture of the catalyst inevitably presents mass transfer resistance. It still remains a grand challenge to open new ways to design and prepare uniform and highly stable supported cluster catalysts under practical catalysis conditions.

Recently, single-atom catalysts become one of the hottest topics due to its unique advantages, such as mechanism studies, cost reduction,

maximum metal utilization, remarkable activity and selectivity [8,9]. Single-atom metal species can aggregate into clusters [10] or larger nanoparticles [11] at elevated temperatures or under reductive atmospheres, which is disadvantaged for their application. However, if using a proper support that suitably interacts with metal species, it is possible to tune the status of active metals from single atoms just into uniform clusters, while not particles, under realistic reaction conditions [12,13]. Thus, it gives us an opportunity to develop a new approach to prepare stable and uniform cluster catalysts with single atoms as precursors.

Supported Ru nanoparticles (> 2 nm) catalysts have widely been used in ammonia decomposition to produce high purity hydrogen for proton exchange membrane fuel cells (PEMFC) [14,15]. They showed the best catalytic activity among the intensively studied active catalysts for ammonia decomposition [16–24]. However, the high loading amount (> 4 wt.%) of Ru [15,16,22] and elevated working temperatures (> 450 °C) [15,17] largely limit its wide application. Stabilized Ru clusters on supports could be a promising candidate to overcome the above drawbacks due to the excellent features of cluster catalysts [1–4]. Among various common oxide supports, nanostructured ceria exhibits

\* Corresponding authors.

E-mail addresses: [sirui@sinap.ac.cn](mailto:sirui@sinap.ac.cn) (R. Si), [cma@hnu.edu.cn](mailto:cma@hnu.edu.cn) (C. Ma), [jiacj@sdu.edu.cn](mailto:jiacj@sdu.edu.cn) (C.-J. Jia).

<https://doi.org/10.1016/j.apcatb.2019.118424>

Received 21 January 2019; Received in revised form 4 November 2019; Accepted 11 November 2019

Available online 16 November 2019

0926-3373/ © 2019 Elsevier B.V. All rights reserved.

unique oxygen storage and release capacity [10,25–29], thus helps tuning the interaction with the deposited metals to stabilize them as ultra-fine clusters. However, depositing Ru clusters on CeO<sub>2</sub> for catalytic decomposition of ammonia has been rarely explored [30].

In this study, we have firstly applied a modified colloidal deposition method to prepare Ru single atoms with low loadings (0.3–1.0 wt.%) anchored on CeO<sub>2</sub> nanorods. Then, very stable and uniform Ru clusters (ca. 1.5 nm) were successfully obtained by reducing atomically dispersed Ru atoms under ammonia atmosphere at 550 °C. The supported Ru clusters showed excellent stability and extremely high catalytic activity with at least one-order improvement on the hydrogen formation yield at 450 °C compared with all the previously reported catalysts for ammonia decomposition.

## 2. Experimental

### 2.1. Synthesis of catalysts

Ru colloidal solution was synthesized by a previously reported procedure [31]. Typically, RuCl<sub>3</sub> (0.15 g; Sinopharm) was added into ethylene glycol (C<sub>2</sub>H<sub>6</sub>O<sub>2</sub>, 50 mL; Sinopharm) under stirring. Then, NaOH (0.16 g; Sinopharm) was added into the above solution and continued stirring for 30 min. Subsequently, the salt solution was refluxed at 160 °C for 3 h. After that, the dark brown solution containing Ru colloids was formed and referred to as Ru colloidal solution.

CeO<sub>2</sub> nanorod (CeO<sub>2</sub>) was synthesized by a known hydrothermal method [32]. Firstly, NaOH (14.40 g; Sinopharm) and Ce(NO<sub>3</sub>)<sub>2</sub>·6H<sub>2</sub>O (1.30 g; kermel) were dissolved in deionized water (40 mL and 20 mL), respectively. Subsequently, the two solutions were mixed into a 100-mL Teflon bottle and kept stirring for 30 min. Finally, the Teflon bottle was sealed into a stainless steel vessel autoclave tightly and heated at 100 °C for 24 h. The resulting precipitates were collected and washed with deionized water and anhydrous ethanol for several times, followed by drying in an oven at 60 °C for 16 h to obtain the final CeO<sub>2</sub> support.

CeO<sub>2</sub> nanosphere (CeO<sub>2</sub>-NS) was synthesized by hydrothermal method reported previously [28]. Typically, Ce(NO<sub>3</sub>)<sub>3</sub>·6H<sub>2</sub>O (2.0 g) was dissolved in Millipore water (18.25 MΩ, 2 mL). Then, acetic acid (C<sub>2</sub>H<sub>4</sub>O<sub>2</sub>, 2 mL; Sinopharm) and glycol (C<sub>2</sub>H<sub>6</sub>O<sub>2</sub>, 52 mL; Sinopharm) were added into the above solution with vigorous stirring for 30 min. The mixture was transferred to a 100-mL Teflon-lined stainless steel autoclave and heated at 180 °C for 200 min. The obtained products were separated and washed with Millipore water and ethanol several times, followed by drying at 75 °C for 10 h. Finally, the product was calcined in air at 400 °C for 1 h.

MgO support was synthesized via thermal decomposition of MgC<sub>2</sub>O<sub>4</sub>·2H<sub>2</sub>O according to the reference [33].

The mesoporous Al<sub>2</sub>O<sub>3</sub> support was prepared according to a previous procedure [34]. Pluronic P123 (M<sub>av</sub> = 5800, EO<sub>20</sub>PO<sub>70</sub>EO<sub>20</sub>, 4.0 g) was dissolved in ethanol (80 mL) at room temperature under stirring. Then, citric acid (C<sub>6</sub>H<sub>8</sub>O<sub>7</sub>, 3.4 g), Al(NO<sub>3</sub>)<sub>3</sub>·9H<sub>2</sub>O (15.0 g) were added into the above solution under vigorous stirring for another 5 h. Subsequently, the mixture was dried at 60 °C for two days. After aging, the as-obtained product was transferred into a tube furnace and calcined in air at 400 °C for 4 h with a slow ramping rate of 1 °C min<sup>-1</sup>.

A series of Ru/CeO<sub>2</sub> catalysts were synthesized according to a modified colloid deposition method [31]. In a typical procedure, the prepared CeO<sub>2</sub> supports (0.5 g) were suspended in Millipore water (12.5 mL). Then, a certain volume of the Ru colloidal solution was added into the above solution under vigorous stirring. After 48 h, the desired samples were separated and washed several times with Millipore water, followed by drying at 60 °C for 48 h. Then, the obtained products were calcined in flowing air at 300 °C for 1 h. Finally, the samples were reduced under ammonia atmosphere at 550 °C. In this work, the catalysts were denoted as xRu/CeO<sub>2</sub> (x = 0.3, 0.6, 1.0), where x is the weight fraction of ruthenium in cerium oxide. In addition, Ru colloidal solution was also deposited on the other three

supports (CeO<sub>2</sub>-NS, MgO, Al<sub>2</sub>O<sub>3</sub>) using the same method. The obtained samples were referred to as 1.0Ru/CeO<sub>2</sub>-NS and 1.0Ru/MgO, 1.0Ru/Al<sub>2</sub>O<sub>3</sub>.

The 1.0Ru/CeO<sub>2</sub>-I samples were prepared by the conventional wetness impregnation method. Typically, the prepared CeO<sub>2</sub> supports (0.4 g) were suspended in Millipore water. Then, a certain volume of the RuCl<sub>3</sub> aqueous solution was added into the above solution under vigorous stirring. After 5 h, the sample was collected by evaporation, followed by drying at 60 °C for 12 h. Finally, the obtained products were calcined in flowing air at 450 °C for 4 h.

### 2.2. Characterization of catalysts

Inductively coupled plasma atomic emission spectroscopy (ICP-AES) analysis of the ruthenium content was determined on an IRIS Intrepid II XSP instrument (Thermo Electron Corporation).

The aberration-corrected high-angle annular dark-field scanning transmission electron micrograph (HAADF-STEM) was obtained using a JEOL ARM200 F microscope equipped with a probe-forming spherical-aberration corrector. The semi-convergence angle is about 24 mrad, and the inner and outer angles of the detector are 90 and 370 mrad, respectively. The average size of Ru species was analyzed on the basis of the statistics of over 100 clusters. The dispersion of Ru species (*D*) was calculated according to the equation [29,35]:  $D = 1.29/d$ , where *d* is the mean particle size (nm) of active metal.

The nitrogen adsorption-desorption test was operated at –196 °C on a Builder SSA-4200 unit. Prior to testing, each sample was degassed at 200 °C for 400 min under vacuum. The specific surface area (*S*<sub>BET</sub>) was calculated according to the Brunauer, Emmett and Teeler (BET) method.

The powder X-ray diffraction (XRD) was carried out on a PANalytical X'Pert<sup>3</sup> powder diffractometer performing in reflection mode with Cu Kα radiation ( $\lambda = 1.5418 \text{ \AA}$ , 40 kV, 40 mA).

The *ex-situ* Raman spectrum was acquired by excitation of the sample at 473 nm using a Raman microscope system (HORIBA Jobin Yvon, LabRAM HR800) in the spectral window with the scanning range from 300 to 1000 cm<sup>-1</sup> (spectral resolution of 2 cm<sup>-1</sup>). The *in-situ* Raman spectrum was obtained from the same instrument with an *in-situ* reaction chamber. Samples were loaded and treated with various atmospheres during the heating and cooling process. Before the test, each sample was pretreated in air (30 mL min<sup>-1</sup>) at 300 °C for 30 min. The data were collected to analyze structure of samples with an acquisition time of 15 min.

X-ray absorption fine structure (XAFS) spectrum at Ru K-edge ( $E_0 = 22117 \text{ eV}$ ) was performed at BL14W1 beamline [36] of Shanghai Synchrotron Radiation Facility (SSRF) operated at 3.5 GeV under “top-up” mode with a constant current of 220 mA. The XAFS data were recorded under fluorescence mode with standard Lytle ion chamber. The absorption edges of Ru foil and RuO<sub>2</sub> were used to calibrate the energy. To avoid the reoxidation of the activated and used samples by exposed to air, we tried to transfer these powders in glove box and sealed them with Kapton films in Ar before the XAFS measurements. The data were extracted and the profiles were fitted according to Athena and Artemis codes. For the X-ray absorption near edge structure (XANES) part, background subtraction and normalization procedures were used to process the experimental absorption coefficients as function of energies  $\mu(E)$ , which was reported as “normalized absorption”. Based on the normalized XANES profiles, the molar fraction of Ru<sup>4+</sup>/Ru<sup>0</sup> can be determined by the linear combination fit [37] with the help of various references (Ru foil for Ru<sup>0</sup> and RuO<sub>2</sub> for Ru<sup>4+</sup>). For the extended X-ray absorption fine structure (EXAFS) part, the Fourier transformed (FT) data in R space were analyzed by applying first shell approximation for the Ru-O shell. The parameters describing the electronic properties (e.g., correction to the photoelectron energy origin,  $E_0$ ) and local structure environment including bond distance (*R*), coordination number (CN), and Debye Waller factor ( $\sigma^2$ ) around the absorbing atom

were allowed to vary during the fit process. The fitted ranges for  $k$  and  $R$  spaces were selected to be  $k = 3\text{--}11 \text{ \AA}^{-1}$  with  $R = 1.0\text{--}3.0 \text{ \AA}$  ( $k^3$  weighted). Since the coordination number (CN) is strongly correlated to Debye-Waller factor in EXAFS fitting, we fixed the Debye-Waller factors for Ru-O and Ru-Ru shells in order to obtain the relatively reliable fitting results on CN. The fixed Debye-Waller factors for Ru-O and Ru-Ru shells were originated from the fully reduced (Ru foil) and fully oxidized references (RuO<sub>2</sub>), respectively.

X-ray photoelectron spectroscopy (XPS) was measured on an Axis Ultra XPS spectrometer (Kratos, UK) with 225 W of Al K $\alpha$  radiation. The C1s signal at 284.6 eV was used to calibrate the binding energy of all spectra.

Temperature programmed reduction by hydrogen (H<sub>2</sub>-TPR) was conducted on a Builder PCSA-1000 instrument (Beijing, China) with a thermal conductivity detector (TCD). Before the test, the as-prepared sample (30 mg) was pretreated in pure O<sub>2</sub> (30 mL min<sup>-1</sup>) at 300 °C for 30 min. Then, the catalyst was heated from room temperature to 400 °C (5 °C min<sup>-1</sup>) in 5 % H<sub>2</sub>/Ar (30 mL min<sup>-1</sup>) gas mixture. The hydrogen consumption was estimated by TCD.

Temperature programmed surface reaction (TPSR) measurement of sample was performed at a mass spectrometer (TILON GRP TECHNOLOGY LIMITED, LC-D200 M). Before measurement, the fresh sample (50 mg, 20–40 mesh) was pretreated in pure NH<sub>3</sub> (19 mL min<sup>-1</sup>) at 550 °C for 1 h. After cooling down, the measured sample was heated from 100 °C to 300 °C with a step of 50 °C in continuous pure NH<sub>3</sub> flow. The signals of NH<sub>3</sub> ( $m/z = 17$ ), H<sub>2</sub> ( $m/z = 2$ ) and N<sub>2</sub> ( $m/z = 28$ ) were tracked during the investigation.

Temperature programmed desorption by ammonia (NH<sub>3</sub>-TPD) of the samples was performed at the same mass spectrometer (TILON GRP TECHNOLOGY LIMITED, LC-D200 M). Before each measurement, the fresh sample (300 mg, 20–40 mesh) was pretreated in 10 % NH<sub>3</sub>/Ar (30 mL min<sup>-1</sup>) gas mixture at 550 °C for 30 min. After cooling down, the measured sample was purged with 10 % NH<sub>3</sub>/Ar (30 mL min<sup>-1</sup>) gas mixture at room temperature for 50 min to obtain saturated adsorption. Subsequently, the feed gas was switched to pure He (30 mL min<sup>-1</sup>) until the stabilization of baseline. Finally, the sample was heated from room temperature to 600 °C (10 °C min<sup>-1</sup>) in pure He (30 mL min<sup>-1</sup>) and the corresponding TPD curve was recorded.

*In-situ* diffuse reflectance infrared Fourier transform spectroscopy (*In-situ* DRIFTS) was carried out in the reaction cell (Harrick) equipped with CaF<sub>2</sub> windows on a Bruker Vertex 70 FTIR spectrometer with a mercury-cadmium-telluride (MCT) detector. DRIFTS tests probed by NH<sub>3</sub> were conducted at a temperature range between 50 and 300 °C with steady-state mode in this work. Prior to test, the fresh samples were subjected to 5 % H<sub>2</sub>/Ar treatment at 550 °C for 1 h. For a typical steady-state mode, the sample was treated in the reaction cell with 5 % H<sub>2</sub>/Ar at 300 °C. Then, the gas mixture (10 % NH<sub>3</sub> in Ar) was prepared with 10 mL min<sup>-1</sup> passing through the catalyst bed for 20 min from 50 °C to 300 °C with a step of 50 °C. The raw spectra were recorded with an acquisition time of 30 s at a resolution of 4 cm<sup>-1</sup>. *In-situ* DRIFTS measurement probed by CO was conducted at 20 °C with steady-state mode. The used samples were subjected to NH<sub>3</sub> treatment in the reaction cell at 300 °C. Subsequently, the sample was purged with helium for 50 min at 300 °C. After cooling down to 20 °C, the gas mixture (2 % CO in Ar) was prepared with 30 mL min<sup>-1</sup> passing through the catalyst bed for 30 min. The spectra were recorded with an acquisition time of 30 s at a resolution of 4 cm<sup>-1</sup>.

Calculations methods. Spin polarized calculations were carried out using the Vienna Ab initio Simulation Package [38–41]. The geometric structures were optimized within the Perdew-Burke-Ernzerhof (PBE) exchange-correlation functional as well as the Projector Augmented-Wave (PAW) pseudopotentials [41–43]. Cut-off energy for plane wave basis was 400 eV. The convergence threshold of the electronic self-consistency was specified to 0.01 meV, and the total energy change between two ionic relaxation steps was designated 0.02 eV. The cleaved CeO<sub>2</sub> (111) surface was comprised of a six-layer slab (Ce 2 layers and O

4 layers) as well as a vacuum layer of 15 Å. In order to accurately describe the Ce 4f orbitals, a Hubbard U term (DFT + U) was involved in the first-principle computations, and the value of U was scaled to 4.5 eV in accordance with previous research [44–46]. The Brillouin zone of the constructed (3 × 3 × 1) supercell was sampled with the k-points (2 × 2 × 1). The interaction between ceria and Ru was simulated with Ru<sub>8</sub> (two layers) lying on the CeO<sub>2</sub> (111) supercell.

### 2.3. Catalytic tests

The catalyst was loaded in a quartz tube fixed-bed reactor with an inner diameter of 6 mm and pure gaseous NH<sub>3</sub> was introduced into the catalyst bed at atmospheric pressure. In order to eliminate the temperature and concentration gradient, 50 mg of the catalyst (20–40 mesh) was mixed with 0.6 g of inert quartz sand (20–40 mesh) and then packed into the reactor. Prior to the catalytic test, the catalyst was activated by pure NH<sub>3</sub> at 550 °C. For the temperature-dependent conversion tests of ammonia decomposition, the reactor temperature was increased from 300 to 550 °C with a step of 50 °C. The concentrations of outlet gases (N<sub>2</sub> and NH<sub>3</sub>) were analyzed by an online gas chromatograph (Ouhua GC 9160). To assess the long-term stability of the catalyst, the reaction temperature was maintained at 450 °C for 48 h and 168 h, respectively. The apparent activation energy for ammonia decomposition was determined with an equal conversion of 12.5 % by tuning the flow rate and temperature.

## 3. Results and discussion

The aberration-corrected high-angle annular dark-field scanning transmission electron micrograph (HAADF-STEM) images show that the obtained Ru colloid possesses two types of Ru species: atomically dispersed species and clusters ca. 1.2 nm (Figure S1). The obtained Ru colloid was deposited on CeO<sub>2</sub> nanorods support. Subsequently, the samples underwent calcination at 300 °C in flowing air to disperse the Ru species [47] (named as 1.0Ru/CeO<sub>2</sub>-Fresh, Table S1). The HAADF-STEM images demonstrate that no Ru clusters or particles were observed, indicating the presence of only atomically dispersed Ru species on the surface of ceria nanorods for the fresh sample (Fig. 1a and Figure S2a, c). Notably, some darker spots can be observed within the ceria nanorods, which results from vacancy of ceria [48]. Very high dispersion of Ru on CeO<sub>2</sub> support is also evidenced by the absence of any Ru-containing phases in X-ray diffraction (XRD, Figure S3). Guided by *ex-situ* X-ray absorption near edge spectroscopy (*ex-situ* XANES) profiles of Ru K-edge result (Fig. 1c), the edge configuration of fresh 1.0Ru/CeO<sub>2</sub> is identical to that of RuO<sub>2</sub>, suggesting its oxidized Ru(IV) nature. This is also confirmed by the X-ray photoelectron spectroscopy (XPS) result (Figure S4a). The corresponding *ex-situ* extended X-ray absorption fine structure (*ex-situ* EXAFS) data in R space determines the only Ru-O shell at ~2 Å (Fig. 1d, Table 1), indicating the sole existence of isolated Ru single atoms, which is well in consistent with the HAADF-STEM result.

As an attractive storage media for hydrogen, ammonia has received extraordinary interest [49] due to the safe storage and transportation. The catalytic decomposition of NH<sub>3</sub> to produce H<sub>2</sub> is very attractive for applications of hydrogen on line [14,15]. Here, the fresh catalyst was activated by pure NH<sub>3</sub> at 550 °C before the catalytic test (named as 1.0Ru/CeO<sub>2</sub>-Activation). Unexpectedly, we obtained uniform and thermally stable Ru clusters supported on CeO<sub>2</sub>. The Ru clusters about 1.5 nm were directly observed in the HAADF-STEM images (Fig. 1b, Figure S2b, d and Figure S5), suggesting that atomically dispersed Ru species were transformed into uniform clusters after NH<sub>3</sub> activation. Notably, the contrast of Ru species is very weak and no lattice fringes were observed in the HAADF-STEM images. The edge jump and profile configuration of *ex-situ* XANES are between Ru foil and RuO<sub>2</sub> reference, revealing the reduction from Ru(IV) to Ru(0) during NH<sub>3</sub> activation (Fig. 1c). The spectra at the K-edge of Ru in k-space where the fitted ranges were selected to be  $k = 3 - 11 \text{ \AA}^{-1}$  ( $k^3$  weighted) show that

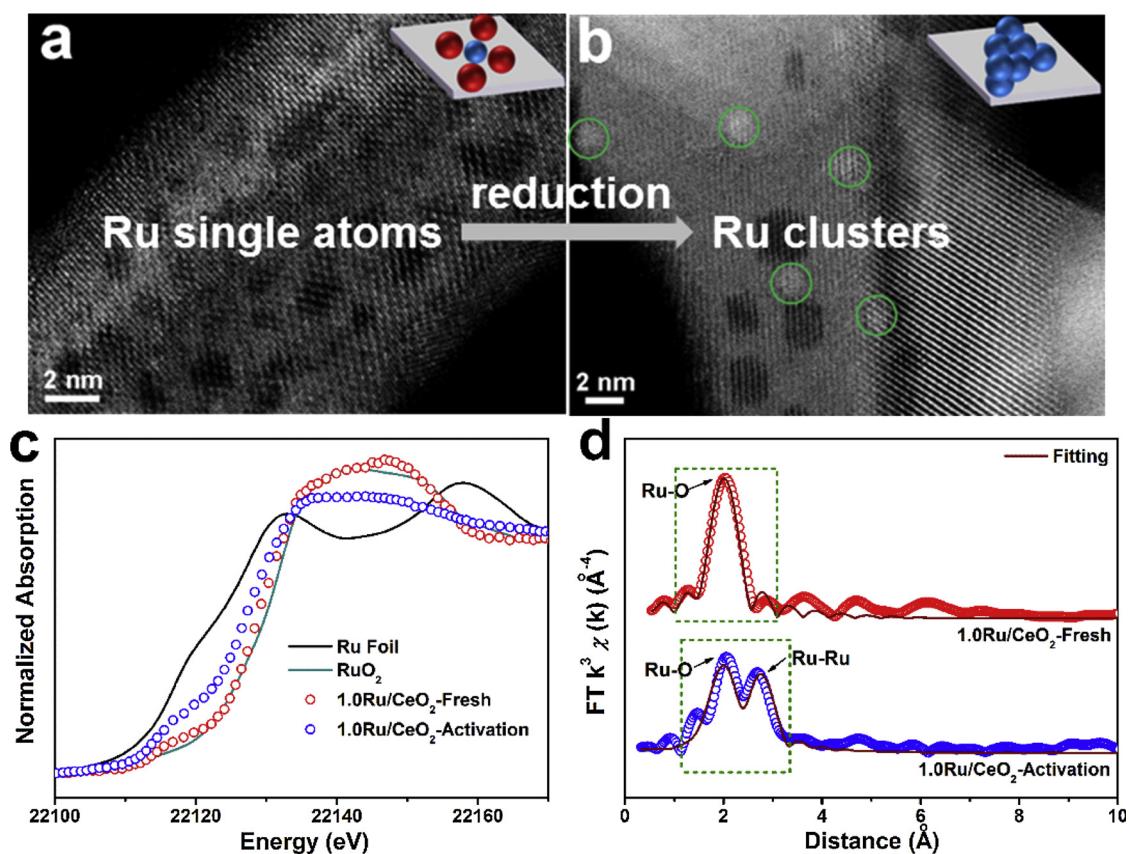


Fig. 1. The aberration-corrected HAADF-STEM images of the 1.0Ru/CeO<sub>2</sub> catalysts: (a) fresh; (b) after NH<sub>3</sub> activation. Green circles: typical Ru clusters. Schematic description of Ru single atoms and Ru clusters as inset. (c) *ex-situ* XANES profiles and (d) *ex-situ* EXAFS spectra of the 1.0Ru/CeO<sub>2</sub> catalysts.

1.0Ru/CeO<sub>2</sub>-Activation is different to that of 1.0Ru/CeO<sub>2</sub>-Fresh (Figure S6). Meanwhile, obvious contribution in *ex-situ* EXAFS spectrum for 1.0Ru/CeO<sub>2</sub>-Activation appears as Ru-Ru metallic bond at ca. 2.7 Å (Fig. 1d, Table 1), which well correlates the XPS results (Figure S4a). It is worth noting that the Ru-O shell still remained, which is caused by the oxidation of Ru clusters by air. However, due to the low concentration of Ru and the severe obstruction from fluorescence of cerium, as well as the form of loose powders under *in-situ* experiment further decreased the Ru signal-to-noise level, the *in-situ* X-ray absorption fine structure (XAFS) measurements cannot provide reliable structural evolution during ammonia decomposition in this work.

The ruthenium species investigated by both XAFS and HAADF-STEM underwent a partial re-oxidation process after the NH<sub>3</sub>-activation. Thus, the 1.5 nm clusters observed in HAADF-STEM are actually composed by a mixture of metallic Ru and ionic Ru<sup>3+</sup> species. We have run linear combination fit on the corresponding XANES profile with the aids of Ru foil and RuO<sub>2</sub> standards, and determined the average oxidation state as +2.0 (50 % Ru and 50 % RuO<sub>2</sub>). If estimating from the relationship between coordination number (CN) and the average size, firstly, we need to adjust the contribution of Ru-Ru shell (fraction: 50 %; CN: 2.4), partial metallic Ru component, to a full metallic Ru

component (assuming 100 %, and thus CN is 4.8), which correlates an average size as ~1 nm, on the basis of previous report on Pt metal [50], considering the similar bond distance between Pt-Pt (2.76 Å) and Ru-Ru (2.70 Å). However, since another 50 % fraction of ruthenium is consisted by Ru<sup>4+</sup> (RuO<sub>2</sub>)-like species, we further used a correction factor of 1.6 (Ru metal: 14.0 Å<sup>3</sup>/atom<sub>Ru</sub>; RuO<sub>2</sub>: 31.4 Å<sup>3</sup>/atom<sub>Ru</sub>; 50 % Ru metal + 50 % RuO<sub>2</sub>) to calculate the average size of ruthenium species. Therefore, according to the EXAFS fitting results, we have identified the average size of our ruthenium clusters to be 1.6 nm, in good agreement with the related HAADF-STEM data (1.5 ± 0.3 nm). It indicates that no significant fraction of isolated Ru species was found for the NH<sub>3</sub>-activated sample.

To explore the transformation from Ru single atoms to metallic Ru clusters, temperature programmed reduction by hydrogen (H<sub>2</sub>-TPR, Fig. 2a) measurement for fresh sample was carried out. We found that the atomically oxidized Ru species were completely reduced below 150 °C, accompanied by a large amount of H<sub>2</sub> consumption, corresponding to the removal of surface oxygen in CeO<sub>2</sub> around Ru species [35,51]. To detect the specific structure of Ru species, Raman technique was used. The *ex-situ* Raman spectra (Fig. 2b) exhibit three new peaks at 830, 703 and 967 cm<sup>-1</sup> for fresh 1.0Ru/CeO<sub>2</sub> with pure CeO<sub>2</sub> as

Table 1  
*Ex-situ* XANES analysis and *ex-situ* EXAFS fitting results.

Catalysts	Ru-O		Ru-Ru		$\sigma^2$ (Å <sup>2</sup> )	$\Delta E_0$ (eV)
	R (Å)	CN	R (Å)	CN		
1.0Ru/CeO <sub>2</sub> (Fresh)	1.99 ± 0.02	4.1 ± 0.4	—	—	0.003 (O)	13.5 ± 2.7
1.0Ru/CeO <sub>2</sub> (Activation)	2.05 ± 0.02	2.3 ± 0.4	2.70 ± 0.02	2.4 ± 0.4	0.006 (Ru)	12.1 ± 2.6
1.0Ru/CeO <sub>2</sub> (Used)	2.03 ± 0.02	2.3 ± 0.4	2.69 ± 0.02	2.3 ± 0.4		12.3 ± 2.6

R: distance; CN: coordination number;  $\sigma^2$ : Debye-Waller factor;  $\Delta E_0$ : correction to the photoelectron energy origin.

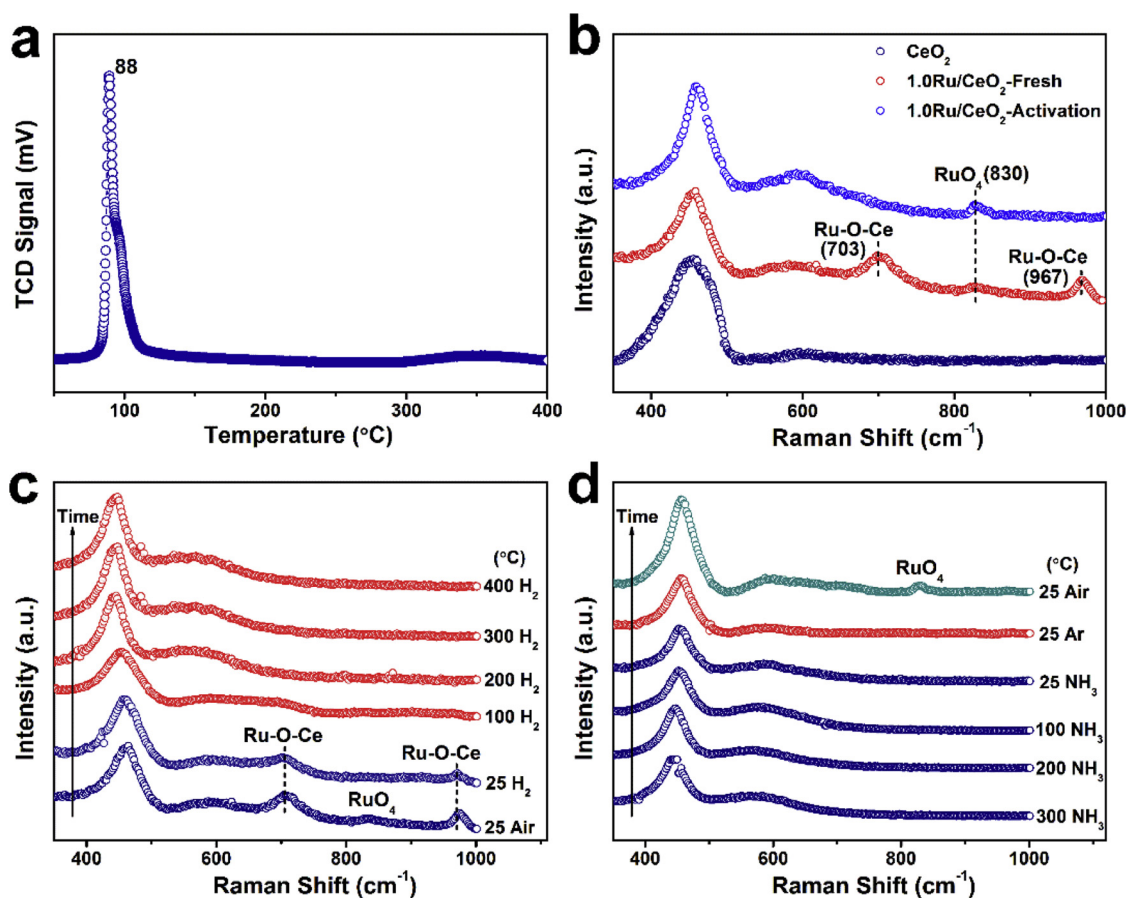


Fig. 2. (a)  $H_2$ -TPR profile of the fresh 1.0Ru/CeO<sub>2</sub> catalyst. (b) *Ex-situ* Raman spectra of the 1.0Ru/CeO<sub>2</sub> catalyst before and after  $NH_3$  activation. *In-situ* Raman spectra of the fresh 1.0Ru/CeO<sub>2</sub> catalyst: (c) under the  $H_2$ -TPR condition; (d) during the  $NH_3$  activation.

reference, which are attributed to Ru(IV)O<sub>4</sub> peroxide species [51–53] and Ru-O-Ce band resulting from the strong interaction between Ru species and CeO<sub>2</sub> [25,35,51], respectively. However, after  $NH_3$  activation, only the RuO<sub>4</sub> species were determined, which is due to the re-oxidation of metallic Ru clusters by air. The Ru-O-Ce structure cannot be recovered by exposing metallic Ru cluster to air at room temperature. To obtain deep insights into the transformation of Ru species during the reduction process, *in-situ* Raman tests were performed (Fig. 2c). First, after oxygen pre-treatment at 300 °C, both Ru-O-Ce structure and RuO<sub>4</sub> species were observed. As 5 %  $H_2$ /Ar was injected, the Raman signals for RuO<sub>4</sub> rapidly vanished at 25 °C, indicating the fast conversion between Ru(IV) and Ru(0). The signals for Ru-O-Ce structure disappeared above 100 °C, in good accordance with the reduction of strongly bound Ru species in the  $H_2$ -TPR test. Similarly, the RuO<sub>4</sub> species and Ru-O-Ce structure were not detectable during the ammonia activation (Fig. 2d). Once the air was injected at room temperature, the RuO<sub>4</sub> species were recovered immediately, confirming the easy oxidation of Ru species in Ru/CeO<sub>2</sub> catalyst.

The catalytic performance of the pre-activated 1.0Ru/CeO<sub>2</sub> sample was evaluated in  $NH_3$  decomposition. The catalyst shows outstanding catalytic activity and excellent long-term stability (Fig. 3a, Table 2 and Figure S7a). The  $H_2$  formation yield reaches 9,924 mmol $H_2$  g<sub>Ru</sub><sup>-1</sup> min<sup>-1</sup> at 450 °C, which is 15 and 33 times of those for well-known active Ru/MgO [17] and Ru/CNTs [15], respectively (Fig. 3a). Also, this value is more than an order of magnitude higher than any other Ru- and transition metal-based catalysts ever reported (Table 2). Especially, the  $H_2$  formation yield for 1.0Ru/CeO<sub>2</sub> reaches about 814 mmol $H_2$  g<sub>Ru</sub><sup>-1</sup> min<sup>-1</sup> even at 350 °C, which is comparable to that of the reported very active Ru/MgO catalyst at 450 °C (631 mmol $H_2$  g<sub>Ru</sub><sup>-1</sup> min<sup>-1</sup>). It is noted that the mass transfer limitation was

eliminated at high GHSV values as shown in Figure S8. The supported Ru cluster catalysts show much higher TOF value for decomposition of ammonia compared with the previously reported results as well (Table 2). In addition,  $NH_3$  conversion during a 168-h test displays nearly constant values of ca. 70 % for  $NH_3$  conversion at 450 °C (Fig. 3a). Meanwhile, the xRu/CeO<sub>2</sub> catalysts with decreasing Ru contents ( $x = 0.3, 0.6$ ) also show prominent activity and stability (Fig. 4a and Table S1). No deactivation is observed during a 48-h test at 450 °C with a very high GHSV of 124,000 cm<sup>3</sup> g<sub>cat</sub><sup>-1</sup> h<sup>-1</sup>. In addition, for the low loading samples, the induction period is much longer than that of the high loading samples (Fig. 4a), due to the stronger interaction between Ru species and support. Besides, we have also prepared the 1.5Ru/CeO<sub>2</sub> catalyst as the theoretical loading of Ru is ca. 1.5 wt.% using the same colloidal deposition method. However, the actual Ru content is ca. 1.09 wt.% (similar to that for the 1.0Ru/CeO<sub>2</sub> catalyst) based on the ICP result (Table S1), lower than that of the theoretical value. It might be attributed to that the surface state of the support has changed during the deposition of the Ru colloid so that the ruthenium loadings were limited, leading to some weight loss of the Ru species with the higher Ru contents compared with the feed intake. The apparent activation energy ( $E_a$ ) values for the xRu/CeO<sub>2</sub> catalysts are almost equal (Fig. 4b), indicating that these catalysts provide the same active sites and follow the similar reaction mechanism. The  $E_a$  values are ca. 150 kJ mol<sup>-1</sup>, which is much higher than the literature data (ca. 70 kJ mol<sup>-1</sup>) reported for other Ru-based catalysts [15,17,22]. The difference on  $E_a$  values was mainly due to the different test methods rather than the reaction conditions, the reaction pathways, particle size or supports [15].

We further characterized the 1.0Ru/CeO<sub>2</sub> catalyst after the ammonia decomposition reaction (named as 1.0Ru/CeO<sub>2</sub>-Used). The

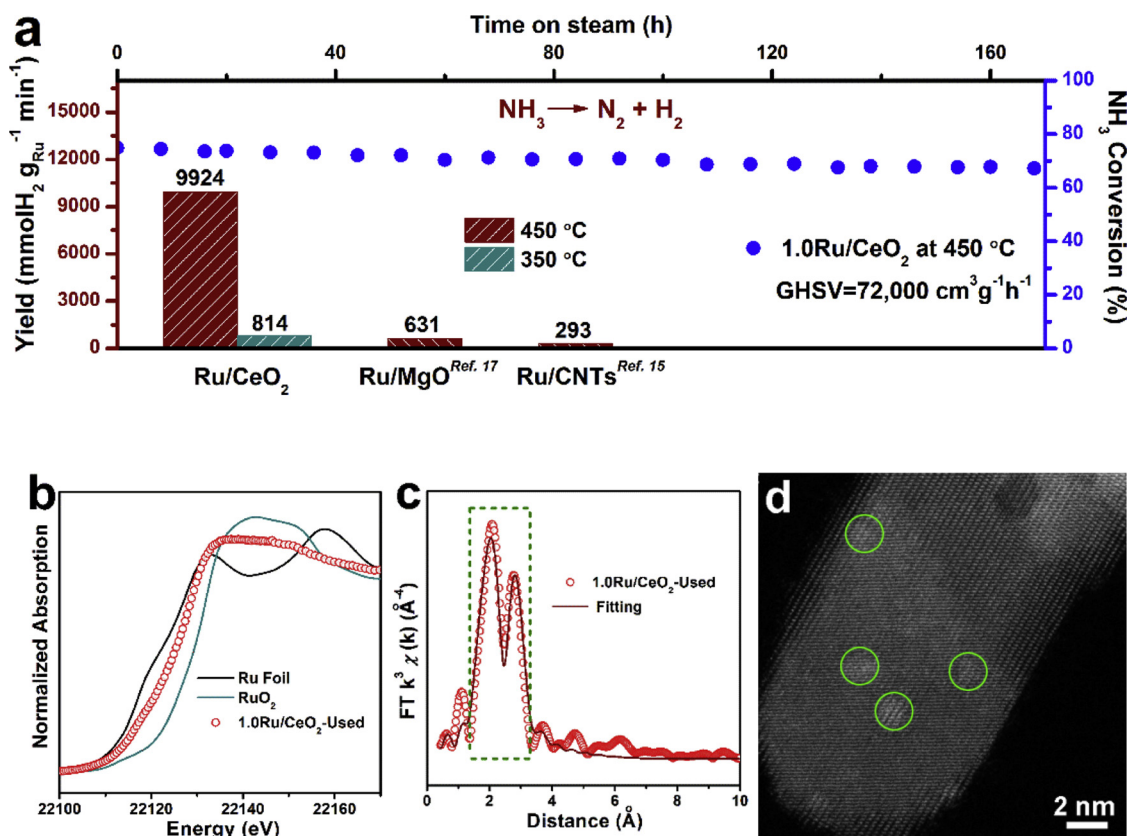


Fig. 3. (a) Comparison of H<sub>2</sub> formation yields (mmolH<sub>2</sub> g<sub>Ru</sub><sup>-1</sup> min<sup>-1</sup>) over 1.0Ru/CeO<sub>2</sub> catalyst and Ru/MgO, Ru/CNTs catalysts from Ref. 17, Ref. 15 at 450 °C and 350 °C and the long-term stability of the 1.0Ru/CeO<sub>2</sub> catalyst tested for 168 h at 450 °C. Structure characterizations of the used catalysts: (b) *ex-situ* XANES profiles; (c) *ex-situ* EXAFS spectra and the fitting range in R space of EXAFS spectra in the dashed box; (d) aberration-corrected HAADF-STEM image.

divergence in *ex-situ* XANES and *ex-situ* EXAFS characterizations both 1.0Ru/CeO<sub>2</sub>-Used and 1.0Ru/CeO<sub>2</sub>-Activation is ignored (Fig. 3b, c and Figure S6, Table 1). Since the CN values of Ru-Ru, as well as the fraction of metallic Ru, in both activated and used catalysts are almost identical (2.4 vs 2.3; 50 % vs 50 %), the same situation appeared for the

estimation of cluster size for the sample after ammonia decomposition reaction. *In-situ* DRIFTS spectrum of CO adsorption was used to probe the surface structure of the used 1.0Ru/CeO<sub>2</sub> catalysts. As shown in Figure S9, the bridge-bonded CO, [Ru<sub>2</sub><sup>0</sup>-(CO)] (1984 cm<sup>-1</sup>) and linear CO adsorption (Ru<sup>0</sup>-CO) (2055 cm<sup>-1</sup> and 2014 cm<sup>-1</sup>) [54,55] were

Table 2

Comparison of catalytic activity over various catalysts from ammonia decomposition.

Catalysts	Metal loading (wt.%)	Temperature (°C)	GHSV (NH <sub>3</sub> cm <sub>3</sub> g <sub>cat</sub> <sup>-1</sup> h <sup>-1</sup> )	Yield (mmolH <sub>2</sub> g <sub>Ru</sub> <sup>-1</sup> min <sup>-1</sup> )	TOF <sub>H<sub>2</sub></sub> (s <sup>-1</sup> ) <sup>b</sup>	Reference
Ru/CeO <sub>2</sub>	1.0	450	228,000	9,924	–	This study
Ru/CeO <sub>2</sub>	1.0	450	124,000	8,303	–	This study
Ru/CeO <sub>2</sub>	1.0	340	110,000	1,618	3.2	This study
Ru/CeO <sub>2</sub>	1.0	350	22,000	814	–	This study
Ru/CeO <sub>2</sub>	1.0	300	22,000	203	–	This study
Ru/MgO	1.0	350	22,000	254	0.6	This study
Ru/MgO	1.0	450	22,000	1,857	–	This study
Ru/Al <sub>2</sub> O <sub>3</sub>	1.1	350	22,000	83	0.2	This study
Ru/CeO <sub>2</sub> -I	1.0	400	22,000	91	–	This study
K-Ru/MgO <sup>d</sup>	3.5	450	36,000	1,125	–	This study
K-Ru/MgO	3.5	450	36,000	998	–	[17]
Ru/MgO	3.5	450	100,000	893	–	[17]
Ru/MgO	2.1	450	36,000	631	–	[17]
Ru/MgO	2.1	350	36,000	96	0.6	[17]
Ru/CNTs	5.0	450	30,000	293	–	[15]
Ru/CNTs	5.0	350	30,000	42	0.3	[15]
Ru/Al <sub>2</sub> O <sub>3</sub>	4.0	450	12,000	301	–	[16]
Ru/Ca(NH <sub>2</sub> ) <sub>2</sub>	10	400	3,000	33	–	[24]
Ru-Cs/graphitized CNT	6.7	400	5,200	87	–	[22]
MnN-2Li <sub>2</sub> NH	43.3	450	60,000	51	–	[19]
Plasma + Co/fumed SiO <sub>2</sub>	27.7	450	2,727	11	–	[20]

<sup>a</sup>The catalyst was synthesized according to Ref. [17] and tested following the same reaction conditions in our reactor. <sup>b</sup>TOF<sub>H<sub>2</sub></sub>: turnover frequency values calculated based on H<sub>2</sub> formation yield at a low NH<sub>3</sub> conversion below 15 %.

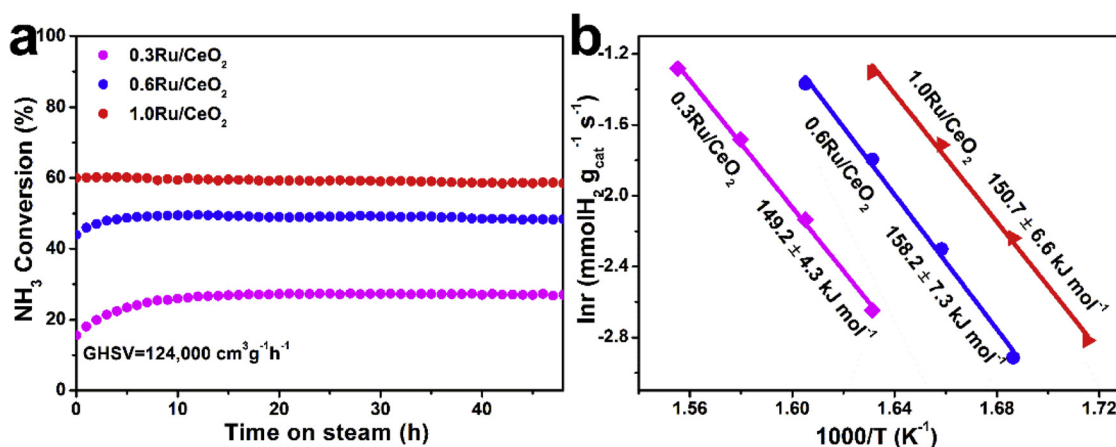


Fig. 4. (a) The long-term stability of the catalysts tested at 450 °C with a GHSV of 124,000 cm<sup>3</sup> g<sub>cat</sub><sup>-1</sup> h<sup>-1</sup> over the xRu/CeO<sub>2</sub> catalysts with different Ru contents (x = 0.3, 0.6, 1.0). (b) The apparent activation energy (E<sub>a</sub>) and the corresponding E<sub>a</sub> value over the catalysts.

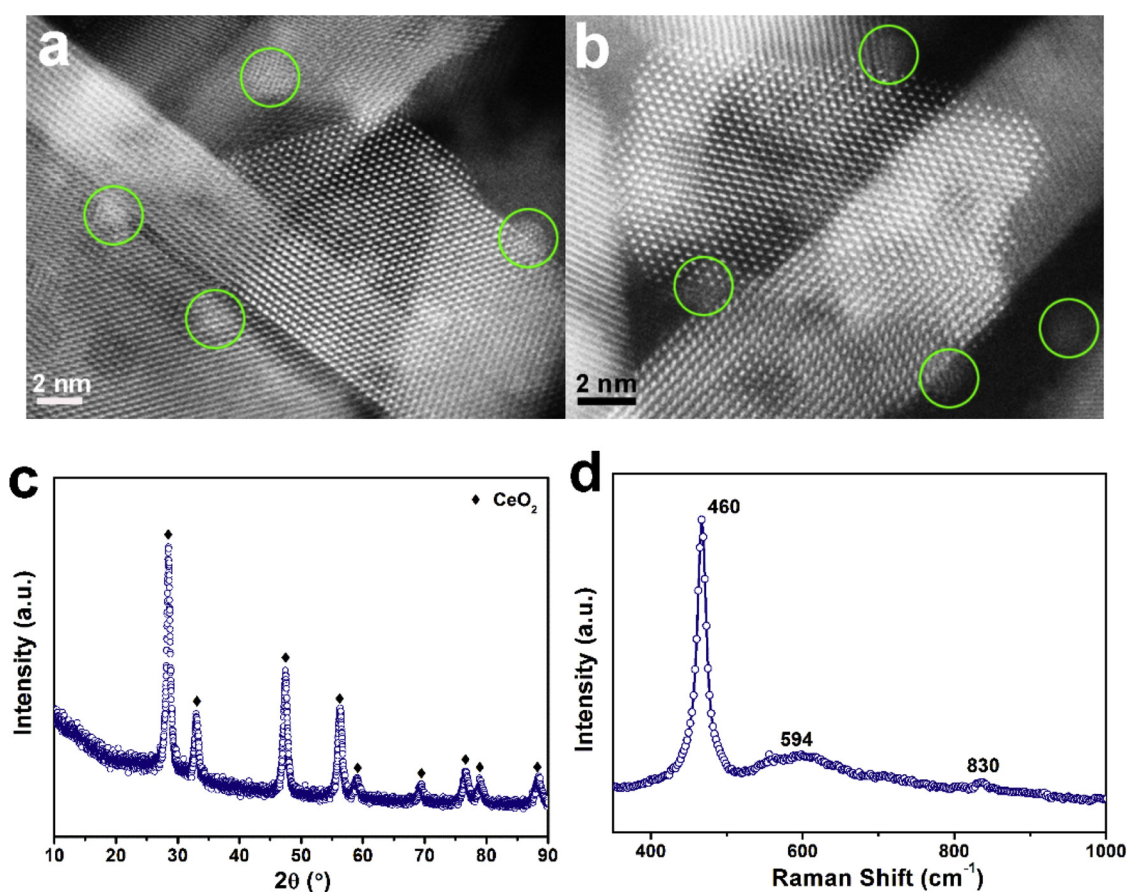


Fig. 5. (a, b) The aberration-corrected HAADF-STEM images of the 1.0Ru/CeO<sub>2</sub> catalyst after the 168 h test. (c) XRD pattern of the 1.0Ru/CeO<sub>2</sub> catalyst after the 168 h test. (d) Raman spectrum of the 1.0Ru/CeO<sub>2</sub> catalyst after the 168 h test.

observed, indicating that the Ru clusters exist in the form of fully metallic state during ammonia decomposition reaction. Moreover, the Ru species were still uniformly dispersed as clusters (ca. 1.5 nm, dispersion of 86 %) in 1.0Ru/CeO<sub>2</sub>-Used (Fig. 3d and Figure S7c), even after a long-term test (Fig. 5a, b). Besides, the XRD and Raman characterization results (Fig. 5c, d) for the 1.0Ru/CeO<sub>2</sub> catalyst after the 168 h test are similar to the results of the used 1.0Ru/CeO<sub>2</sub> sample, demonstrating the remarkable anti-sintering ability of the Ru/CeO<sub>2</sub> catalysts.

The 1.0Ru/CeO<sub>2</sub> catalyst shows excellent low-temperature catalytic reactivity as well, while CeO<sub>2</sub> itself as support does not contribute to the activity (Fig. 6a). Ammonia conversion drastically increases with the

elevation of reaction temperature and the H<sub>2</sub> formation yield reaches 203 mmolH<sub>2</sub> g<sub>Ru</sub><sup>-1</sup> min<sup>-1</sup> at 300 °C for 1.0Ru/CeO<sub>2</sub> (Table 2). Notably, the catalytic activity of the 1.0Ru/CeO<sub>2</sub>-Fresh (not pre-activated) catalyst is somehow lower than that of the 1.0Ru/CeO<sub>2</sub> catalyst after the activation below 400 °C (Fig. 6a), while the catalytic activity of both catalysts is similar above 400 °C, revealing the reduction from Ru(IV) to Ru(0) during NH<sub>3</sub> activation below 400 °C. In addition, temperature programmed surface reaction (TPSR, Fig. 6b) experiment displays that signals of H<sub>2</sub> and N<sub>2</sub> are detected even at very low temperatures (> 100 °C), indicating the superior activation of ruthenium clusters for ammonia decomposition.

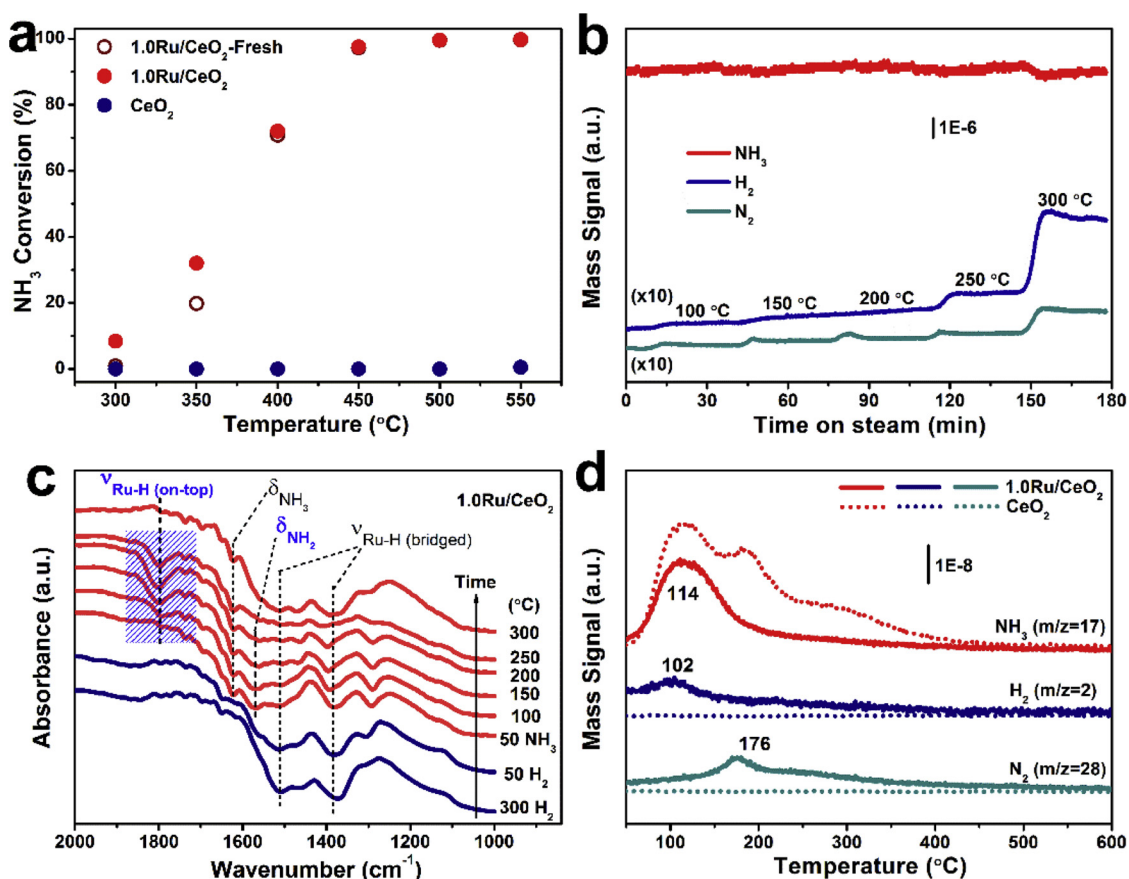


Fig. 6. (a) Temperature-dependent NH<sub>3</sub> conversion with a GHSV of 22,000 cm<sup>3</sup> g<sub>cat</sub><sup>-1</sup> h<sup>-1</sup> over the 1.0Ru/CeO<sub>2</sub>-Fresh, 1.0Ru/CeO<sub>2</sub> and CeO<sub>2</sub> samples. (b) TPRS on 1.0Ru/CeO<sub>2</sub> based on the ammonia decomposition reaction. (c) *In-situ* DRIFTS study of NH<sub>3</sub> adsorption on 1.0Ru/CeO<sub>2</sub> during the heating process. (d) NH<sub>3</sub>-TPD profiles of CeO<sub>2</sub> and 1.0Ru/CeO<sub>2</sub>.

The operando information of the intrinsic active species for ammonia decomposition is significantly important, while rarely concerned in reported work. Thus, *in-situ* DRIFTS measurement under ammonia atmosphere was implemented in this work. As shown in Fig. 6c and Figure S10, Table S2, after pre-activation of the fresh catalysts in 5 % H<sub>2</sub>/Ar, once 10 % NH<sub>3</sub>/Ar was introduced into the reactor at 50 °C, the adsorption of coordinated ammonia was immediately observed on both pure CeO<sub>2</sub> and 1.0Ru/CeO<sub>2</sub>. Further, the on-top Ru-H (1800 cm<sup>-1</sup>) [56] and NH<sub>2</sub> species (1573 cm<sup>-1</sup>) [57,58] appeared on 1.0Ru/CeO<sub>2</sub> at 100 °C, suggesting that decomposition of NH<sub>3</sub> could occur at very low temperature over the 1.0Ru/CeO<sub>2</sub> catalyst. In addition, with the elevating test temperature, the intensity of on-top Ru-H band first increased and then decreased, finally disappeared at 300 °C (Fig. 6c), at which gaseous hydrogen was significantly produced (Fig. 6b). Meanwhile, the NH<sub>2</sub> species gradually decreased, confirming that NH<sub>2</sub> species are easy to be further decomposed. Notably, the bridging Ru-H bands (1508 and 1380 cm<sup>-1</sup>) [56] were also observed for 1.0Ru/CeO<sub>2</sub>, which resulted from the pre-treatment of the sample under 5 % H<sub>2</sub>/Ar atmospheres, suggesting that the bridging Ru-H bands are more related to the activation of H<sub>2</sub> molecule, not the intermediates to produce H<sub>2</sub> from NH<sub>3</sub>. From the *in-situ* DRIFTS results, we identified the on-top Ru-H and NH<sub>2</sub> species on the catalysts surface as the active intermediates. Temperature programmed desorption by ammonia (NH<sub>3</sub>-TPD; Fig. 6d) results exhibit that CeO<sub>2</sub> support itself has good NH<sub>3</sub> adsorption ability. Meanwhile, Ru/CeO<sub>2</sub> catalyst can facilitate the dissociation adsorption of NH<sub>3</sub> as products of H<sub>2</sub> and N<sub>2</sub> below 200 °C, which is well consistent with the results of TPRS.

To further confirm the advantage of the Ru cluster catalyst for catalytic decomposition of ammonia, the 1.0Ru/CeO<sub>2</sub>-I sample was prepared via conventional wetness impregnation method. The HAADF-

STEM images showed that no Ru clusters were observed on the surface of CeO<sub>2</sub> for the used 1.0Ru/CeO<sub>2</sub>-I catalyst because the Ru is lighter than Ce (Figure S11). Even so, Ru species still existed as metallic Ru clusters, due to the easy reducibility of the Ru species in high-temperature reduction reaction (Figure S9 and Figure S12). The catalytic performance of the 1.0Ru/CeO<sub>2</sub>-I catalyst is much lower than that of the 1.0Ru/CeO<sub>2</sub> catalyst (Fig. 7a, Table 2), suggesting the importance of catalyst preparation method. Although the adsorption ability of NH<sub>3</sub> for 1.0Ru/CeO<sub>2</sub>-I and 1.0Ru/CeO<sub>2</sub> samples is similar, the N<sub>2</sub> signals appear at higher temperature for 1.0Ru/CeO<sub>2</sub>-I samples compared with that for 1.0Ru/CeO<sub>2</sub> (Fig. 7b). In addition, H<sub>2</sub>-TPR results showed that the reduction temperature of Ru species for 1.0Ru/CeO<sub>2</sub>-I catalyst was much higher (100–220 °C) compared with that (70–120 °C) for the 1.0Ru/CeO<sub>2</sub> catalyst (Figure S12), confirming that the active Ru species in the 1.0Ru/CeO<sub>2</sub>-I catalyst were not easier to be reduced, leading to the lower catalytic activity. Besides, the difference in activity between 1.0Ru/CeO<sub>2</sub> and 1.0Ru/CeO<sub>2</sub>-I could also be attributed to the particle size of Ru species, which can influence the number of surface B5 sites [16]. Therefore, the uniform and stable Ru clusters by reducing the Ru single atoms can be a highly efficient supported catalyst for catalytic decomposition of ammonia to hydrogen.

To better understand whether or not the morphology of ceria influences the catalytic activity, we synthesized 1.0Ru/CeO<sub>2</sub>-NS catalyst with CeO<sub>2</sub> spheres as supports. The activity of the 1.0Ru/CeO<sub>2</sub>-NS catalyst is comparable to that of the 1.0Ru/CeO<sub>2</sub> catalyst (Fig. 8a). The Ru species can also exist predominantly as ca. 1.5 nm clusters on CeO<sub>2</sub> nanospheres after the catalytic test (Fig. 8b). The XRD and TPR results (Fig. 8c, d) for the 1.0Ru/CeO<sub>2</sub>-NS catalyst are analogous to those of the 1.0Ru/CeO<sub>2</sub>. These results demonstrate the morphology of CeO<sub>2</sub> support does not have influence on the catalytic activity, indicating there is

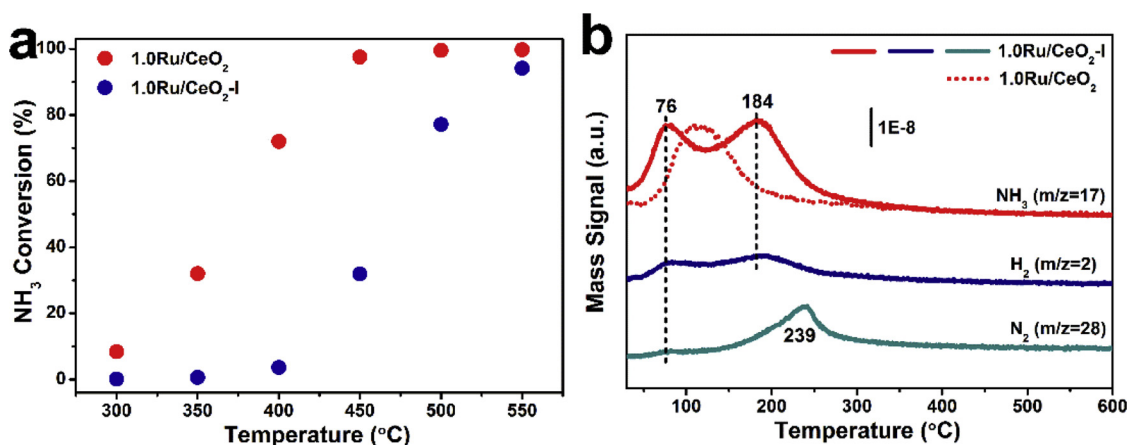


Fig. 7. (a) Temperature-dependent NH<sub>3</sub> conversion for the 1.0Ru/CeO<sub>2</sub> and 1.0Ru/CeO<sub>2</sub>-I catalysts with a GHSV of 22,000 cm<sup>3</sup> g<sub>cat</sub><sup>-1</sup> h<sup>-1</sup>. (b) NH<sub>3</sub>-TPD profiles of the 1.0Ru/CeO<sub>2</sub>-I catalyst.

no obvious surface plane effect to the ceria support in the Ru/CeO<sub>2</sub> catalyst. This may be attributed to the surface structure reconstruction [27,28] of CeO<sub>2</sub> nanorods from {110}/{100} to the most stable {111}, making two supports exhibit similar activity.

Besides, we resorted to spin polarized density functional theory (DFT) calculations using the Vienna Ab initio Simulation Package [38,40] to investigate the NH<sub>3</sub> decomposition reaction pathway on 1.0Ru/CeO<sub>2</sub>. The surface was constructed by docking the Ru<sub>8</sub> cluster in the CeO<sub>2</sub> (111) surface, followed by two competing reaction pathways

(Figure S13). The adsorption energy of NH<sub>3</sub> on Ce-site (-0.77 eV) is a little less favorable than that on Ru-site (-0.97 eV) of constructed surface. However, the consequent dehydrogenation of adsorbed NH<sub>3</sub> (NH<sub>3</sub>→NH<sub>2</sub>+H) on Ce-site is much more unfavorable compared with that on Ru-site (0.33 eV v.s. -0.43 eV), although the H atoms in the adsorbed NH<sub>3</sub> are close enough to be captured by Ru cluster. NH<sub>3</sub> decomposition mainly occurs on Ru clusters through consecutive dehydrogenation steps. Therefore, the adsorption of NH<sub>3</sub> on Ce-site could only help the mass transfer, while does not contribute directly to the

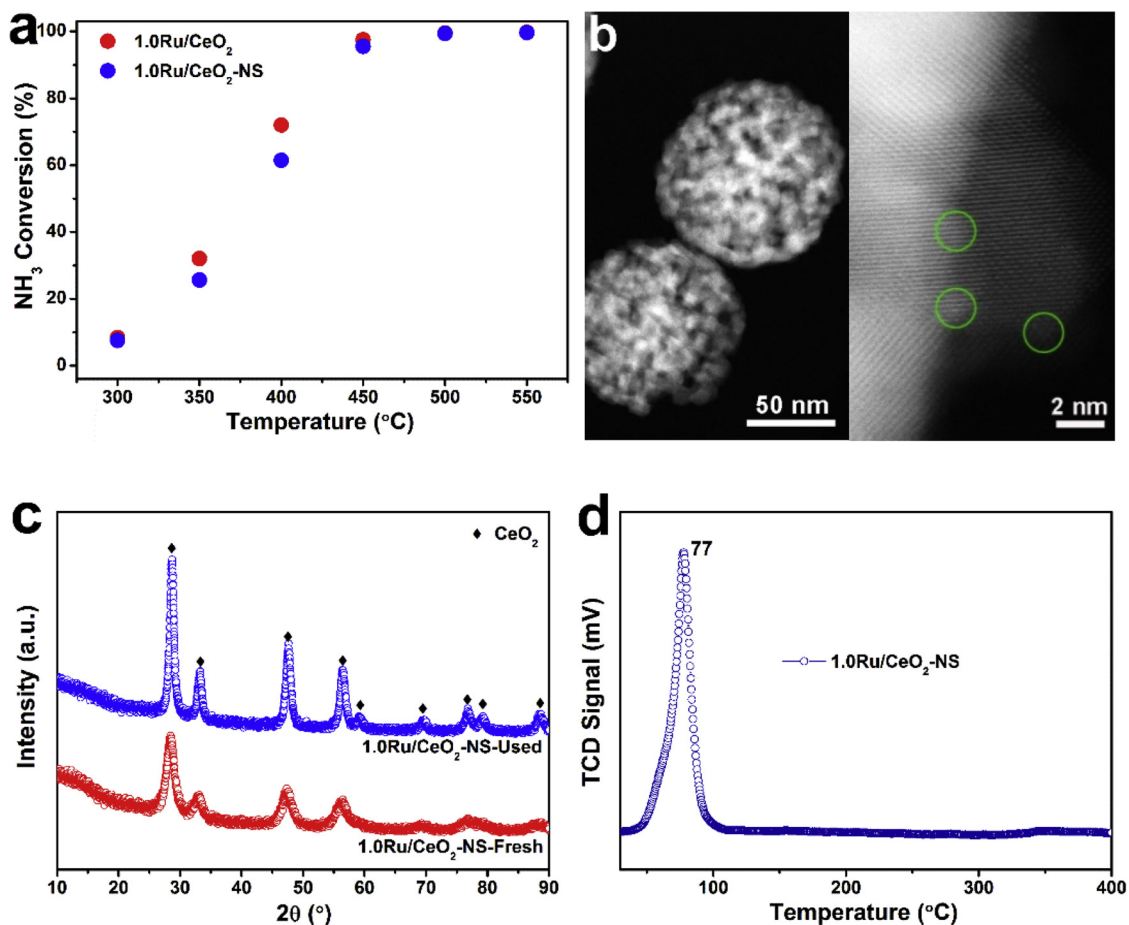
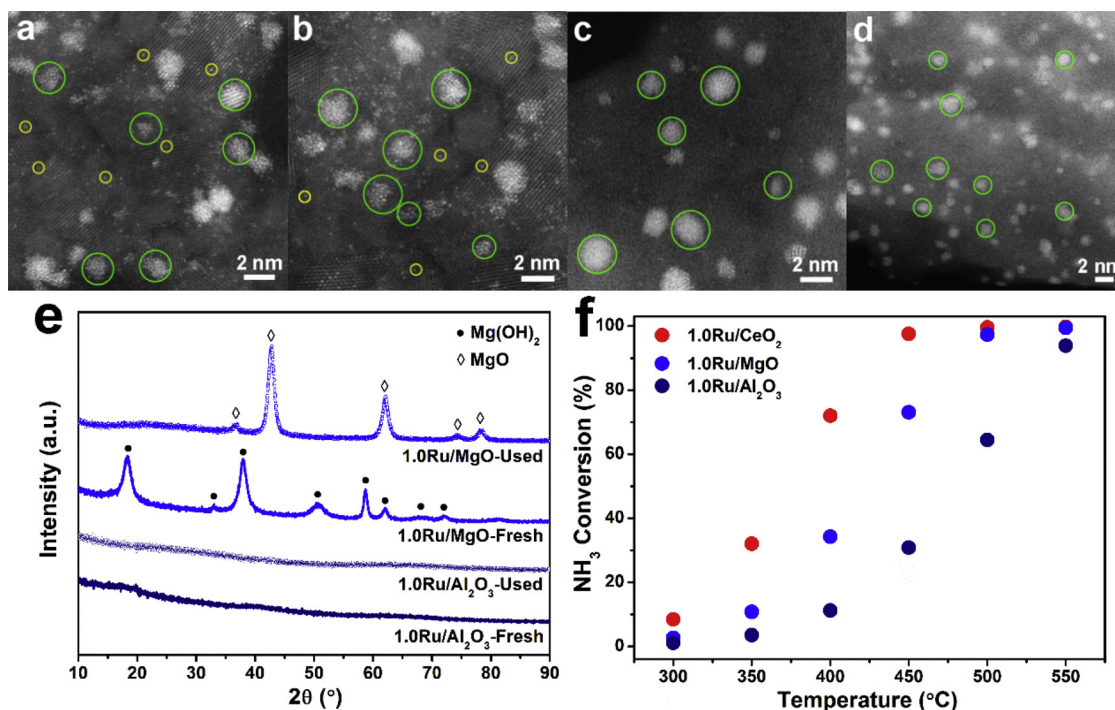
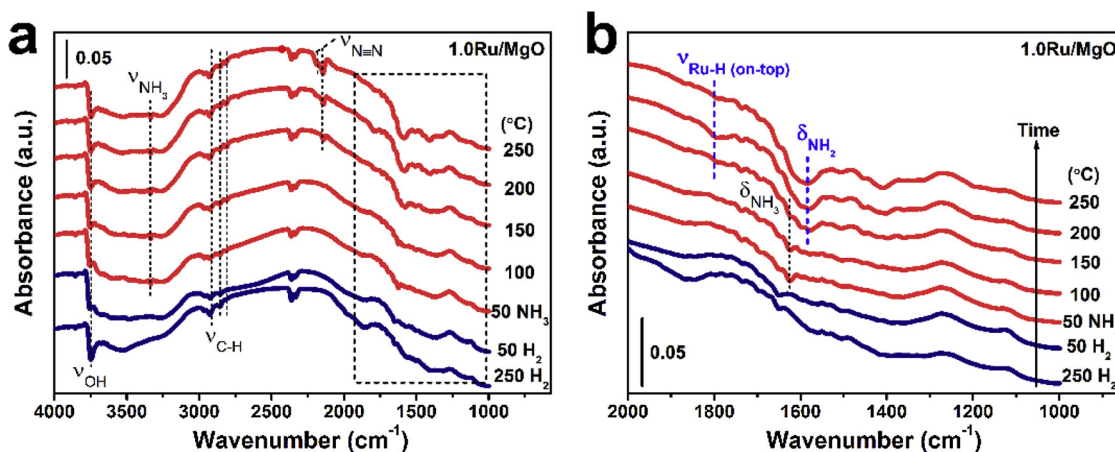


Fig. 8. (a) Temperature-dependent NH<sub>3</sub> conversion with a GHSV of 22,000 cm<sup>3</sup> g<sub>cat</sub><sup>-1</sup> h<sup>-1</sup> over the 1.0Ru/CeO<sub>2</sub> and 1.0Ru/CeO<sub>2</sub>-NS catalysts. (b) The aberration-corrected HAADF-STEM images of the used 1.0Ru/CeO<sub>2</sub>-NS catalyst. Green circles: typical Ru clusters. (c) XRD patterns of the fresh and used 1.0Ru/CeO<sub>2</sub>-NS catalysts. (d) H<sub>2</sub>-TPR profile of the fresh 1.0Ru/CeO<sub>2</sub>-NS catalyst.



**Fig. 9.** (a, b) The aberration-corrected HAADF-STEM images of the used 1.0Ru/MgO catalyst. Yellow circles: typical Ru single atoms; green circles: typical Ru clusters. (c, d) The aberration-corrected HAADF-STEM images of the used 1.0Ru/Al<sub>2</sub>O<sub>3</sub> catalyst. Green circle: typical Ru clusters and nanoparticles. (e) XRD patterns of the fresh and used 1.0Ru/MgO and 1.0Ru/Al<sub>2</sub>O<sub>3</sub> catalysts. (f) Temperature-dependent NH<sub>3</sub> conversion for 1.0Ru/MgO, 1.0Ru/Al<sub>2</sub>O<sub>3</sub> and 1.0Ru/CeO<sub>2</sub> catalysts with a GHSV of 22,000 cm<sup>3</sup> g<sub>cat</sub><sup>-1</sup> h<sup>-1</sup>.



**Fig. 10.** (a) *In-situ* DRIFTS study of NH<sub>3</sub> adsorption on 1.0Ru/MgO during the heating process. (b) The partial enlarged detail of (a) in the dashed box.

dehydrogenation reaction.

In addition, the reference 1.0Ru/MgO and 1.0Ru/Al<sub>2</sub>O<sub>3</sub> catalysts synthesized via the same colloidal deposition approach and tested under the same conditions. On the basis of HAADF-STEM results (Fig. 9a–d), the Ru species mainly exist in the form of both single atoms and ca. 1.6 nm clusters for 1.0Ru/MgO catalysts (Fig. 9a, b and Figure S14a) and both 1.6 nm clusters and ca. 2.2 nm nanoparticles for 1.0Ru/Al<sub>2</sub>O<sub>3</sub> catalysts (mean: 1.7 nm, Fig. 9c, d and Figure S14b). XRD shows that no distinct diffraction peak is attributed to Ru species for all the samples (Fig. 9e), indicating that Ru species are dispersed highly on the surface of the support. This observation is in accordance with HAADF-STEM result (Fig. 9a–d). Here, the 1.0Ru/MgO catalyst exhibits much higher H<sub>2</sub> yield than the same chemical composition samples synthesized by other approaches (Table 2), demonstrating the importance of catalyst preparation method. On the other hand, 1.0Ru/MgO catalyst is clearly less active than 1.0Ru/CeO<sub>2</sub>. While, the performance of the

1.0Ru/Al<sub>2</sub>O<sub>3</sub> catalyst is much lower than the other two catalysts (Fig. 9f, Table 2).

The evolution on surface species of 1.0Ru/MgO during ammonia decomposition was investigated by *in-situ* DRIFTS (Fig. 10). After 10 % NH<sub>3</sub>/Ar was introduced into the reactor at 50 °C, the adsorption of ammonia was immediately observed. Further, the on-top Ru-H (1800 cm<sup>-1</sup>) [56], dinitrogen molecules (2194 and 2146 cm<sup>-1</sup>) [56,58,59] and NH<sub>2</sub> species (1586 cm<sup>-1</sup>) [57,58] were present above 200 °C. The dinitrogen molecules and NH<sub>2</sub> species are relatively stable and strongly interact with the surface of oxide matrix, resulting in the relatively lower catalytic activity than ceria-supported ruthenium catalyst. NH<sub>3</sub>-TPD results showed that the adsorption of NH<sub>3</sub> was observed on MgO and Al<sub>2</sub>O<sub>3</sub> supports (Fig. 11a, c). However, the adsorption peak of NH<sub>3</sub> is modified after the introduction of Ru (Fig. 11b, d). Meanwhile, the desorption peaks of H<sub>2</sub> and N<sub>2</sub> are observed. This suggests that Ru species can promote the dissociative adsorption of NH<sub>3</sub>. Compared with

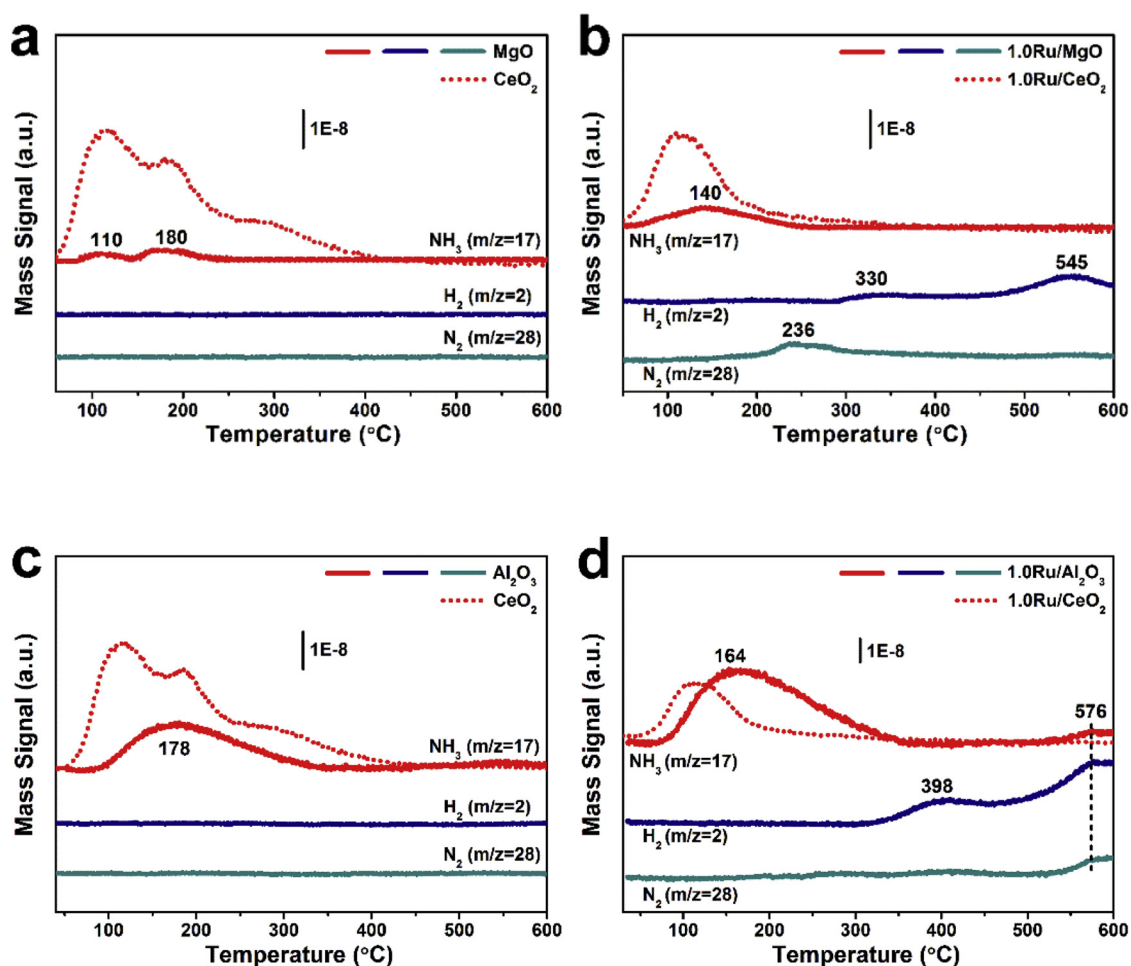


Fig. 11.  $\text{NH}_3$ -TPD profiles of the prepared samples: (a) MgO; (b) 1.0Ru/MgO; (c)  $\text{Al}_2\text{O}_3$ ; (d) 1.0Ru/ $\text{Al}_2\text{O}_3$ .

$\text{CeO}_2$  support and 1.0Ru/ $\text{CeO}_2$  sample, much weaker  $\text{NH}_3$  adsorption was determined for the MgO and  $\text{Al}_2\text{O}_3$  supports and 1.0Ru/MgO samples. Moreover, the  $\text{H}_2$  and  $\text{N}_2$  signals appear at obviously higher temperature for 1.0Ru/MgO and 1.0Ru/ $\text{Al}_2\text{O}_3$  compared with those for 1.0Ru/ $\text{CeO}_2$ , indicating the stronger interaction between  $\text{N}_2$ ,  $\text{H}_2$  and catalyst, leading to the lower catalytic activity. These results suggest that the weak  $\text{NH}_3$  adsorption and the strong interaction between adsorbed species and support surface make against dissociative desorption of  $\text{NH}_3$ , which highlights the crucial importance of ceria support for Ru catalysts.

#### 4. Conclusions

In summary, stable and uniform Ru clusters anchored on nanoceria have been synthesized by reducing isolated Ru single atoms. The Ru cluster catalyst shows unprecedented activity and excellent long-term stability for decomposition of ammonia. The synergistic effect between very good  $\text{NH}_3$  adsorption ability of  $\text{CeO}_2$  and excellent stability of Ru clusters promotes the catalytic performance. This work not only offers guidance for the design of high-efficiency supported cluster catalysts, but also provides a deep understanding for the investigation on structure-activity relation in heterogeneous catalysis.

#### Declaration of Competing Interest

The authors declare no competing financial interest.

#### Acknowledgments

Financial supported from the Excellent Young Scientists Fund from National Science Foundation of China (NSFC) (grant no. 21622106), other projects from the NSFC (grant nos. 21331001, 21773288, 21805167, 11574281 and 21771117), the Outstanding Scholar Fund (grant no. JQ201703) and the Doctoral Fund (grant no. ZR2018BB010) from the Science Foundation of Shandong Province of China, the Taishan Scholar Project of Shandong Province of China, the National Key Basic Research Program of China (2017YFA0403402) and the Future Program for Young Scholars of Shandong University (grant no. 11190089964158). We thank Jun-Xiang Chen, Dao-Lei Wang, and Lu Shen (TILON GRP TECHNOLOGY LIMITED) for their kind help on the mass spectra measurement and data-analysis. We thank the Center of Structural Characterization and Property Measurements at Shandong University for the help on sample characterizations.

#### Appendix A. Supplementary data

Supplementary material related to this article can be found, in the online version, at doi:<https://doi.org/10.1016/j.apcatb.2019.118424>.

#### References

- [1] Y. Lei, F. Mehmood, S. Lee, J. Greeley, B. Lee, S. Seifert, R.E. Winans, J.W. Elam, R.J. Meyer, P.C. Redfern, D. Teschner, R. Schlögl, M.J. Pellin, L.A. Curtiss, S. Vajda, *Science* 328 (2010) 224–228 <http://science.sciencemag.org/content/328/5975/224>.
- [2] K. Judai, S. Abbet, A.S. Wörz, U. Heiz, C.R. Henry, Low-temperature cluster catalysis, *J. Am. Chem. Soc.* 126 (2004) 2732–2737, <https://doi.org/10.1021/>

- ja039037k.
- [3] S. Vajda, M.J. Pellin, J.P. Greeley, C.L. Marshall, L.A. Curtiss, G.A. Ballentine, J.W. Elam, S. Catillon-Mucherie, P.C. Redfern, F. Mehmood, P. Zapol, Subnanometre platinum clusters as highly active and selective catalysts for the oxidative dehydrogenation of propane, *Nat. Mater.* 8 (2009) 213–216 <http://www.nature.com/articles/nmat2384>.
  - [4] A.A. Herzing, C.J. Kiely, A.F. Carley, P. Landon, G.J. Hutchings, Identification of active gold nanoclusters on iron oxide supports for CO oxidation, *Science* 321 (2008) 1331–1335 <http://science.sciencemag.org/content/321/5894/1331>.
  - [5] X. Pan, X. Bao, The effects of confinement inside carbon nanotubes on catalysis, *Acc. Chem. Res.* 44 (2011) 553–562, <https://doi.org/10.1021/ar100160t>.
  - [6] H. Song, R.M. Rioux, J.D. Hoefelmeyer, R. Komor, K. Niesz, M. Grass, P. Yang, G.A. Somorjai, Hydrothermal growth of mesoporous SBA-15 silica in the presence of PVP-Stabilized Pt nanoparticles: synthesis, characterization, and catalytic properties, *J. Am. Chem. Soc.* 128 (2006) 3027–3037, <https://doi.org/10.1021/ja057383r>.
  - [7] P.M. Arnal, M. Comotti, F. Schüth, High-temperature-stable catalysts by hollow sphere encapsulation, *Angew. Chem. Int. Ed.* 45 (2006) 8224–8227, <https://doi.org/10.1002/anie.200603507>.
  - [8] X. Yang, A. Wang, B. Qiao, J. Li, J. Liu, T. Zhang, Single-atom catalysts: a new frontier in heterogeneous catalysis, *Acc. Chem. Res.* 46 (2013) 1740–1748, <https://doi.org/10.1021/ar300361m>.
  - [9] P. Liu, Y. Zhao, R. Qin, S. Mo, G. Chen, L. Gu, D.M. Chevrier, P. Zhang, Q. Guo, D. Zang, B. Wu, G. Fu, N. Zheng, Photochemical route for synthesizing atomically dispersed palladium catalysts, *Science* 352 (2016) 797–801, <https://doi.org/10.1126/science.aae0330>.
  - [10] L.W. Guo, P.P. Du, X.P. Fu, C. Ma, J. Zeng, Contributions of distinct gold species to catalytic reactivity for carbon monoxide oxidation, *Nat. Commun.* 7 (2016) 13481, <https://doi.org/10.1038/ncomms13481> <https://www.nature.com/articles/ncomms13481>.
  - [11] Y. Guo, D. Gu, Z. Jin, P. Du, R. Si, Tao J, W. Xu, Y. Huang, S. Senanayake, Q. Song, C. Jia, F. Schüth, Uniform 2 nm gold nanoparticles supported on iron oxides as active catalysts for CO oxidation reaction: structure–activity relationship, *Nanoscale* 7 (2015) 4920–4928 <https://pubs.rsc.org/en/content/articlehtml/2015/nr/c4nr06967f>.
  - [12] Y. Kim, K. Ohshima, K. Higashimine, T. Uruga, M. Takata, H. Suematsu, T. Mitani, Fine size control of platinum on carbon nanotubes: from single atoms to clusters, *Angew. Chem. Int. Ed.* 45 (2006) 407–411, <https://doi.org/10.1002/anie.200501792>.
  - [13] H. Xiong, S. Lin, J. Goetze, P. Pletcher, H. Guo, L. Kovarik, K. Artyushkova, B.M. Weckhuysen, A.K. Datye, Thermally Stable and Regenerable Platinum-Tin Clusters for Propane Dehydrogenation Prepared by Atom Trapping on Ceria, *Angew. Chem. Int. Ed.* 56 (2017) 8986–8991, <https://doi.org/10.1002/anie.201701115>.
  - [14] F. Schüth, R. Palkovits, R. Schlögl, D.S. Su, Ammonia as a possible element in an energy infrastructure: catalysts for ammonia decomposition, *Energy Environ. Sci.* 5 (2012) 6278–6289 <https://pubs.rsc.org/en/content/articlehtml/2012/ee/c2ee02865d>.
  - [15] S. Yin, Q. Zhang, B. Xu, W. Zhu, C. Ng, C. Au, Investigation on the catalysis of CO<sub>2</sub>-free hydrogen generation from ammonia, *J. Catal.* 224 (2004) 384–396, <https://doi.org/10.1016/j.jcat.2004.03.008>.
  - [16] A.M. Karim, V. Prasad, G. Mpourmpakis, W.W. Loneragan, A.I. Frenkel, Correlating particle size and shape of supported Ru/γ-Al<sub>2</sub>O<sub>3</sub> catalysts with NH<sub>3</sub> decomposition activity, *J. Am. Chem. Soc.* 131 (2009) 12230–12239, <https://doi.org/10.1021/ja902587k>.
  - [17] X. Ju, L. Liu, P. Yu, J. Guo, X. Zhang, T. He, G. Wu, P. Chen, Mesoporous Ru/MgO prepared by a deposition-precipitation method as highly active catalyst for producing CO<sub>2</sub>-free hydrogen from ammonia decomposition, *Appl. Catal. B* 211 (2017) 167–175, <https://doi.org/10.1016/j.apcatb.2017.04.043>.
  - [18] A. Lu, J. Nitz, M. Comotti, C. Weidenthaler, K. Schlichte, C.W. Lehmann, O. Terasaki, F. Schüth, Spatially and size selective synthesis of Fe-based nanoparticles on ordered mesoporous supports as highly active and stable catalysts for Ammonia decomposition, *J. Am. Chem. Soc.* 132 (2010) 14152–14162, <https://doi.org/10.1021/ja105308e>.
  - [19] J. Guo, F. Chang, P. Wang, D. Hu, P. Yu, G. Wu, Z. Xiong, P. Chen, Highly Active MnN-Li<sub>2</sub>NH Composite Catalyst for Producing CO<sub>2</sub>-Free Hydrogen, *ACS Catal.* 5 (2015) 2708–2713, <https://doi.org/10.1021/acscatal.5b00278>.
  - [20] L. Wang, Y. Yi, Y. Zhao, R. Zhang, J. Zhang, H. Guo, NH<sub>3</sub> Decomposition for H<sub>2</sub> Generation: Effects of Cheap Metals and Supports on Plasma-Catalyst Synergy, *ACS Catal.* 5 (2015) 4167–4174, <https://doi.org/10.1021/acscatal.5b00728>.
  - [21] W. Zheng, T.P. Cotter, P. Kaghazchi, T. Jacob, B. Frank, Experimental and theoretical investigation of molybdenum carbide and nitride as catalysts for Ammonia decomposition, *J. Am. Chem. Soc.* 135 (2013) 3458–3464, <https://doi.org/10.1021/ja309734u>.
  - [22] A.K. Hill, L. Torrente-Murciano, Low temperature H<sub>2</sub> production from ammonia using ruthenium-based catalysts: synergetic effect of promoter and support, *Appl. Catal. B* 172–173 (2015) 129–135, <https://doi.org/10.1016/j.apcatb.2015.02.011>.
  - [23] D.A. Hansgen, D.G. Vlachos, J.G. Chen, Using first principles to predict bimetallic catalysts for the ammonia decomposition reaction, *Nat. Chem.* 2 (2010) 484–489 <https://www.nature.com/articles/nchem.626>.
  - [24] K. Kishida, M. Kitano, Y. Inoue, M. Sasase, T. Nakao, T. Tada, H. Abe, Y. Niwa, T. Yokoyama, M. Hara, H. Hosono, Large oblate hemispherical ruthenium particles supported on calcium amide as efficient catalysts for Ammonia decomposition, *Chem. Eur. J.* 24 (2018) 7976–7984, <https://doi.org/10.1002/chem.201800467>.
  - [25] J. An, Y. Wang, J. Lu, J. Zhang, Z. Zhang, S. Xu, X. Liu, T. Zhang, M. Gocyla, M. Heggen, R.E. Dunin-Borkowski, P. Fornasiero, F. Wang, Acid-Promoter-Free Ethylene Methoxycarbonylation over Ru-Clusters/Ceria: The Catalysis of Interfacial Lewis Acid-Base Pair, *J. Am. Chem. Soc.* 140 (2018) 4172–4181, <https://doi.org/10.1021/jacs.8b01742>.
  - [26] F. Wang, S. He, H. Chen, B. Wang, L. Zheng, M. Wei, D.G. Evans, X. Duan, Active Site Dependent Reaction Mechanism over Ru/CeO<sub>2</sub> Catalyst toward CO<sub>2</sub> Methanation, *J. Am. Chem. Soc.* 138 (2016) 6298–6305, <https://doi.org/10.1021/jacs.6b02762>.
  - [27] N. Ta, J.J. Liu, S. Chenna, P.A. Crozier, Y. Li, Stabilized gold nanoparticles on ceria nanorods by strong interfacial anchoring, *J. Am. Chem. Soc.* 134 (2012) 20585–20588, <https://doi.org/10.1021/ja310341j>.
  - [28] W. Wang, W. Yu, P. Du, H. Xu, Z. Jin, R. Si, C. Ma, S. Shi, C. Jia, C. Yan, Crystal Plane Effect of Ceria on Supported Copper Oxide Cluster Catalyst for CO Oxidation: Importance of Metal-Support Interaction, *ACS Catal.* 7 (2017) 1313–1329, <https://doi.org/10.1021/acscatal.6b03234>.
  - [29] Y. Guo, S. Mei, K. Yuan, D. Wang, H. Liu, C. Yan, Y. Zhang, Low-Temperature CO<sub>2</sub> Methanation over CeO<sub>2</sub>-Supported Ru Single Atoms, Nanoclusters, and Nanoparticles Competitively Tuned by Strong Metal-Support Interactions and H-Spillover Effect, *ACS Catal.* 8 (2018) 6203–6215, <https://doi.org/10.1021/acscatal.7b04469>.
  - [30] I. Lucentini, A. Casanovas, J. Llorca, Catalytic ammonia decomposition for hydrogen production on Ni, Ru and Ni-Ru supported on CeO<sub>2</sub>, *Int. J. Hydrogen Energy* (2019), <https://doi.org/10.1016/j.ijhydene.2019.01.154>.
  - [31] H.A.E. Dole, L.F. Safady, S. Ntais, M. Couillard, E.A. Baranova, Electrochemically enhanced metal-support interaction of highly dispersed Ru nanoparticles with a CeO<sub>2</sub> support, *J. Catal.* 318 (2014) 85–94, <https://doi.org/10.1016/j.jcat.2014.07.003>.
  - [32] H. Mai, L. Sun, Y. Zhang, R. Si, W. Feng, H. Zhang, H. Liu, C. Yan, Shape-Selective Synthesis and Oxygen Storage Behavior of Ceria Nanopolyhedra, Nanorods, and Nanocubes, *J. Phys. Chem. B* 109 (2005) 24380–24385, <https://doi.org/10.1021/jp055584b>.
  - [33] H. Guan, P. Wang, H. Wang, B. Zhao, Y. Zhu, Y. Xie, Preparation of nanometer magnetite with high surface area and study on the influencing factors of the preparation process, *Acta Phys.-Chim. Sin.* 22 (2006) 804–808, [https://doi.org/10.1016/S1872-1508\(06\)60033-8](https://doi.org/10.1016/S1872-1508(06)60033-8).
  - [34] Q. Yuan, A. Yin, C. Luo, L. Sun, Y. Zhang, W. Duan, H. Liu, C. Yan, Facile Synthesis for Ordered Mesoporous γ-Alumina with High Thermal Stability, *J. Am. Chem. Soc.* 130 (2008) 3465–3472, <https://doi.org/10.1021/ja0764308>.
  - [35] F. Wang, C. Li, X. Zhang, M. Wei, D.G. Evans, X. Duan, Catalytic behavior of supported Ru nanoparticles on the {100}, {110}, and {111} facet of CeO<sub>2</sub>, *J. Catal.* 329 (2015) 177–186, <https://doi.org/10.1016/j.jcat.2015.05.014>.
  - [36] H. Yu, X. Wei, J. Li, S. Gu, S. Zhang, L. Wang, J. Ma, L. Li, Q. Gao, R. Si, F. Sun, Y. Wang, F. Song, H. Xu, X. Yu, Y. Zou, J. Wang, Z. Jiang, Y. Huang, The XAFS beamline of SSRF, *Nucl. Sci. Technol.* 26 (2015) 050102 <http://www.cqvip.com/qk/85361x/201505/666747245.html>.
  - [37] A.I. Frenkel, Q. Wang, N. Marinkovic, J.G. Chen, L. Barrio, R. Si, A.L. Cámara, A.M. Estrella, J.A. Rodriguez, J.C. Hanson, Combining X-ray absorption and X-ray diffraction techniques for in situ studies of chemical transformations in heterogeneous catalysis: advantages and limitations, *J. Phys. Chem. C* 115 (2011) 17884–17890, <https://doi.org/10.1021/jp205204e>.
  - [38] G. Kresse, J. Hafner, Ab initio molecular dynamics for liquid metals, *Phys. Rev. B* 47 (1993) 558–561, <https://doi.org/10.1103/PhysRevB.47.558>.
  - [39] G. Kresse, J. Hafner, Ab initio molecular-dynamics liquid-metal—amorphous-semiconductor simulation of the transition in germanium, *Phys. Rev. B* 49 (1994) 14251–14269, <https://doi.org/10.1103/PhysRevB.49.14251>.
  - [40] G. Kresse, J. Furthmüller, Efficient iterative schemes for ab initio total-energy calculations using a plane-wave basis set, *Phys. Rev. B* 54 (1996) 11169–11186, <https://doi.org/10.1103/PhysRevB.54.11169>.
  - [41] G. Kresse, D. Joubert, From ultrasoft pseudopotentials to the projector augmented-wave method, *Phys. Rev. B* 59 (1999) 1758–1775, <https://doi.org/10.1103/PhysRevB.59.1758>.
  - [42] J.P. Perdew, K. Burke, M. Ernzerhof, Generalized gradient approximation made simple, *Phys. Rev. Lett.* 77 (1997) 3865–3868, <https://doi.org/10.1103/PhysRevLett.77.3865>.
  - [43] P.E. Blöchl, Projector augmented-wave method, *Phys. Rev. B* 50 (1994) 17953–17979, <https://doi.org/10.1103/PhysRevB.50.17953>.
  - [44] M. Saito, C.A. Roberts, C. Ling, DFT + U Study of the Adsorption and Oxidation of an Iron Oxide Cluster on CeO<sub>2</sub> Support, *J. Phys. Chem. C* 119 (2015) 17202–17208, <https://doi.org/10.1021/acs.jpcc.5b04569>.
  - [45] Y. Liu, H. Li, J. Yu, D. Mao, G. Lu, Electronic storage capacity of ceria: role of peroxide in Au<sub>x</sub> supported on CeO<sub>2</sub> (111) facet and CO adsorption, *Phys. Chem. Phys.* 17 (2015) 27758–27768 <https://pubs.rsc.org/en/content/articlehtml/2015/cp/c5cp03394b>.
  - [46] J. Zhang, X. Gong, G. Lu, Catalytic activities of CeO<sub>2</sub> (110)-2 × 1 reconstructed surface, *Surf. Sci.* 632 (2015) 164–173, <https://doi.org/10.1016/j.susc.2014.10.009>.
  - [47] A. Aitbekova, L. Wu, C.J. Wrasman, A. Boubnov, A.S. Hoffman, E.D. Goodman, S.R. Bare, M. Cargnello, Low-temperature restructuring of CeO<sub>2</sub>-Supported Ru nanoparticles determines selectivity in CO<sub>2</sub> catalytic reduction, *J. Am. Chem. Soc.* 140 (2018) 13736–13745, <https://doi.org/10.1021/jacs.8b07615>.
  - [48] J. Jones, H. Xiong, A.T. DeLaRiva, E.J. Peterson, H. Pham, S.R. Challa, G. Qi, S. Oh, M.H. Wiebenga, X. Hernández, Y. Wang, A.K. Datye, Thermally stable single-atom platinum-on-ceria catalysts via atom trapping, *Science* 353 (2016) 150–154 <https://science.sciencemag.org/content/353/6295/150>.
  - [49] A. Afif, N. Radenahmad, Q. Cheok, S. Shams, J.H. Kim, A.K. Azad, Ammonia-fed fuel cells: a comprehensive review, *Renew. Sustain. Energy Rev.* 60 (2016) 822–835, <https://doi.org/10.1016/j.rser.2016.01.120>.

- [50] A.I. Frenkel, C.W. Hills, R.G. Nuzzo, A view from the inside: complexity in the atomic scale ordering of supported metal nanoparticles, *J. Phys. Chem. B* 105 (2001) 12689–12703, <https://doi.org/10.1021/jp012769j>.
- [51] H. Huang, Q. Dai, X. Wang, Morphology effect of Ru/CeO<sub>2</sub> catalysts for the catalytic combustion of chlorobenzene, *Appl. Catal. B* 158–159 (2014) 96–105, <https://doi.org/10.1016/j.apcatb.2014.01.062>.
- [52] H. Chan, C.G. Takoudis, M.J. Weaver, High-pressure oxidation of ruthenium as probed by Surface-Enhanced Raman and X-Ray photoelectron spectroscopies, *J. Catal.* 172 (1997) 336–345, <https://doi.org/10.1006/jcat.1997.1841>.
- [53] K.S. Joya, H.J.M. de Groot, Electrochemical in situ surface enhanced Raman spectroscopic characterization of a trinuclear ruthenium complex, Ru-red, *J. Raman Spectrosc.* 44 (2013) 1195–1199, <https://doi.org/10.1002/jrs.4329>.
- [54] S.Y. Chin, C.T. Williams, M.D. Amiridis, FTIR studies of CO adsorption on Al<sub>2</sub>O<sub>3</sub>- and SiO<sub>2</sub>-Supported Ru catalysts, *J. Phys. Chem. B* 110 (2006) 871–882, <https://doi.org/10.1021/jp053908q>.
- [55] J. Shen, N. Semagina, Iridium- and Platinum-Free Ring Opening of Indan, *ACS Catal.* 4 (2013) 268–279, <https://doi.org/10.1021/cs400986v>.
- [56] Y. Izumi, K. Aika, Promoted catalysis by supported [Ru<sub>6</sub>N] clusters in N<sub>2</sub> and/or H<sub>2</sub>: structural and chemical controls, *J. Phys. Chem.* 99 (1995) 10346–10353, <https://doi.org/10.1021/j100025a042>.
- [57] L. Zhang, H. He, Mechanism of selective catalytic oxidation of ammonia to nitrogen over Ag/Al<sub>2</sub>O<sub>3</sub>, *J. Catal.* 268 (2009) 18–25, <https://doi.org/10.1016/j.jcat.2009.08.011>.
- [58] G. Ramis, L. Yi, G. Busca, M. Turco, E. Kötur, R.J. Willey, Adsorption, Activation, and Oxidation of Ammonia over SCR Catalysts, *J. Catal.* 157 (1995) 523–532, <https://doi.org/10.1006/jcat.1995.1316>.
- [59] K. Hashimoto, N. Toukai, Decomposition of ammonia over a catalyst consisting of ruthenium metal and cerium oxides supported on Y-form zeolite, *J. Mol. Catal. A Chem.* 161 (2000) 171–178, [https://doi.org/10.1016/S1381-1169\(00\)00332-0](https://doi.org/10.1016/S1381-1169(00)00332-0).